Smart Antenna Configurations – Analysis Based on ESPRIT Methods

Sava Savov[1], Viara Vasileva[2] and Miroslava Doneva[3]

Abstract – **In this paper, the simple direction of arrival (DOA) methods for uniform rectangular array (URA) and uniform circular array (UCA) based on narrowband radio-frequency signals are introduced. Arrays are composed of a number of uniformly distributed identical half-wavelength dipoles. Numerical examples are presented to illustrate these methods.**

Keywords – **Direction of arrival, Half-wavelength dipole, Smart antenna, Uniform circular array, Uniform rectangular array.**

I. Introduction

Smart antennas (adaptive arrays) can provide a substantial capacity improvement in the frequency-resource-limited radio-communication system. They are used in order to improve capacity per user channel and better quality [6].

Spatial processing is the central idea for smart antennas. This is a technology that would be implemented into the existing wireless communications infrastructures to provide broader channel bandwidth and new improved services.

The investigation of smart antennas suitable for wireless communication systems has involved primary uniform circular arrays (UCA) and uniform rectangular arrays (URA). They possess the ability to scan in 3-D space, and it is necessary for wireless devices to scan the main beam in any direction of elevation and azimuth.

Two DOA estimation methods are introduced for the significant improvement in smart antenna resolution [6]. This paper presents UCA-ESPRIT and the 2-D unitary ESPRIT for direction of arrival estimation analysis of UCA and URA, respectively. Limited numerical examples are depicted to illustrate these algorithms.

[1]Sava V. Savov is with Department of Electrical Engineering, Technical University of Varna, 1 Studentska Str., Varna 9010, Bulgaria, Senior Member IEEE
E-mail: savovsv@yahoo.com
[2]Viara Y. Vasileva is with Department of Electrical Engineering, Technical University of Varna, 1 Studentska Str., Varna 9010, Bulgaria,
E-mail: via_vas@abv.bg
[3]Miroslava G. Doneva is with Department of Electrical Engineering, Technical University of Varna, 1 Studentska Str., Varna 9010, Bulgaria,
E-mail: m_grisheva@abv.bg

II. Uniform Circular and Rectangular Array Configurations

A. Circular antenna structure

The UCA with radius a consisting N equally distributed identical half-wavelength dipoles is located on x-y plane, as illustrated in Fig. 1.

An incoming plane wave (narrowband signal) with wavelength λ arrives at the array from elevation angle θ and azimuth angle ϕ. A spherical coordinate system is used to denote the arrival direction. The origin of coordinate system is located at the center of the array.

As presented in Fig. 1, the array factor *(AF)* of UCA is given by [4]

$$AF(\theta,\phi)=\sum_{n=1}^{N} w_n e^{-jka\sin\theta\ \cos(\phi-\phi_n)} \qquad (1)$$

where w_n, $\theta=\pi/2$ and ϕ_n are the estimated weights and angular positions of the nth element, respectively, a is the radius of the UCA, and k is the wave number ($k=2\pi/\lambda$).

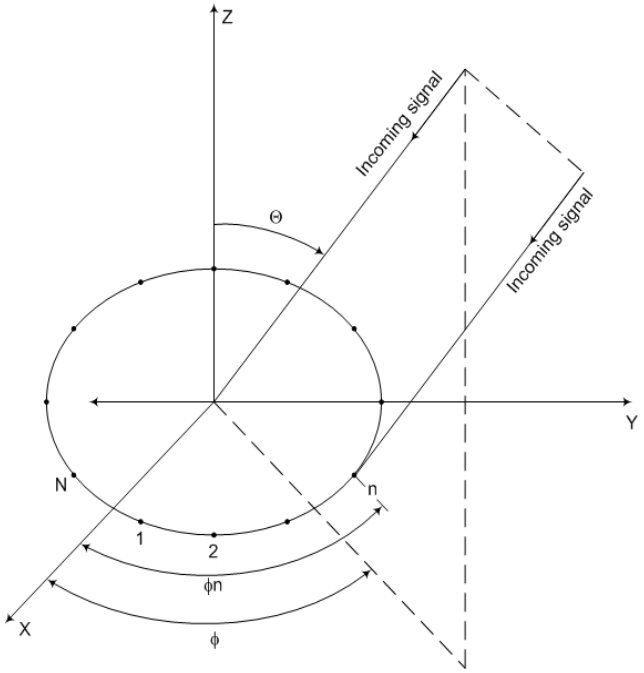

Fig. 1. UCA geometry, along with an incoming plane wave

B. Rectangular antenna structure

The URA consisting N x M equally distributed identical half-wavelength dipoles (M, N – even) is located symmetrical in x-y plane, as illustrated in Fig. 2.

The array factor *(AF)* of URA with its maximum along θ_0, ϕ_0 is given by [3]

$$[\mathrm{AF}(\theta,\phi)]_{\mathrm{MxN}} = 4\sum_{m=1}^{M/2}\sum_{n=1}^{N/2} A_{mn}\cos[(2m-1)u]\cos[(2n-1)v] \quad (2)$$

where

$$u = \frac{\pi d_x}{\lambda}(\sin\theta\cos\phi - \sin\theta_0\cos\phi_0) \quad (3)$$

$$v = \frac{\pi d_y}{\lambda}(\sin\theta\sin\phi - \sin\theta_0\sin\phi_0) \quad (4)$$

and A_{mn} is the amplitude excitation of the individual element, d_x, d_y are the interelement spacing along the x-axis and the y-axis, respectively.

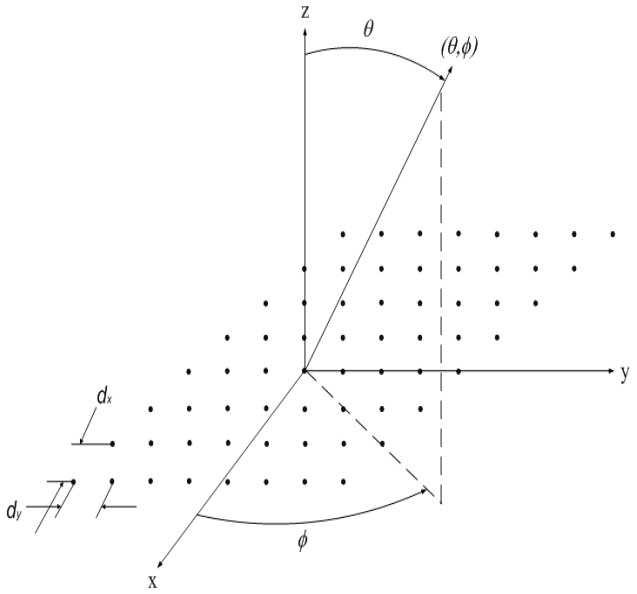

Fig. 2. URA geometry, along with an incoming plane wave

III. DIRECTION OF ARRIVAL ESTIMATION METHODS

A. UCA-ESPRIT method

The UCA-ESPRIT method is unique different from the classical ESPRIT. Applying this algorithm under the conditions of a UCA structure, the eigenvalues of each correlation array matrix have the form [4]

$$\lambda_i = \sin\theta_i e^{j\phi_i} \quad (5)$$

where (θ_i, ϕ_i) are respectively elevation and azimuth angles of incoming plane wave of *i*th signal source ($i = 1,2,...,M$), M is the number of the narrowband sources.

The three basic steps of real valued estimation are [1]:

1. The signal eigenvector estimation.
2. The equation system solution derived from eigenvectors computed in step 1.
3. The eigenvalues estimation of the solution to the system worked out in step 2.

This method gives several advantages in comparison with classical ESPRIT, such as: a) reduced computational complexity; b) very accurate finds simultaneously both the elevation and azimuth angles of arrival for incoming signals, and c) lower SNR (signal-to-noise ratio) resolution thresholds [5].

B. 2-D unitary ESPRIT method

The 2-D unitary ESPRIT algorithm is unique different from the classical ESPRIT, first of them provides closed-form automatically paired two dimensional estimation as long as the elevation and azimuth of each narrowband signal arrives at the URA [1]. Applying this method under the conditions of a URA structure (Fig. 2), the array manifold has the matrix form

$$\mathbf{A}(\mu,\nu) = \mathbf{a}_N(\mu)\mathbf{a}_M^T(\nu) \quad (6)$$

where the array manifold is

$$\mathbf{a}_N(\mu) = \left[e^{-j\left(\frac{N-1}{2}\right)\mu}, \ldots, e^{-j\mu}, 1, e^{j\mu}, \ldots, e^{j\left(\frac{N-1}{2}\right)\mu}\right]^T \quad (7)$$

$$\mu = \frac{2\pi}{\lambda} d_x p \quad (8)$$

λ is the wavelength, p is the direction cosine variable relative to the *x*-axis and

$$\mathbf{a}_M(\nu) = \left[e^{-j\left(\frac{M-1}{2}\right)\nu}, \ldots, e^{-j\nu}, 1, e^{j\nu}, \ldots, e^{j\left(\frac{M-1}{2}\right)\nu}\right]^T \quad (9)$$

is defined from $\mathbf{a}_N(\mu)$ with N, μ replaced by M, ν respectively

$$\nu = \frac{2\pi}{\lambda} d_y q \quad (10)$$

is the spatial frequency variable, q is the direction cosine variable relative to the *y*-axis.

Pre-multiplying $\mathbf{A}(\mu,\nu)$ by $\mathbf{Q}_N^H$ and post-multiplying by $\mathbf{Q}_M^*$, creates the real valued N *x* M array manifold

$$\begin{aligned}\mathbf{D}(\mu,\nu) &= \mathbf{Q}_N^H\mathbf{A}(\mu,\nu)\mathbf{Q}_M^* = \\ &= \mathbf{Q}_N^H\mathbf{a}_N(\mu)\mathbf{a}_M^T(\nu)\mathbf{Q}_M^* = \mathbf{d}_N(\mu)\mathbf{d}_M^T(\nu)\end{aligned} \quad (11)$$

where $\mathbf{Q}_N^H$, $\mathbf{Q}_M^H$ are a sparse unitary matrices that transforms $\mathbf{a}_N(\mu)$ into an N *x 1* real valued vector manifold

$$\mathbf{d}_N(\mu) = \mathbf{Q}_N^H\mathbf{a}_N(\mu) \quad (12)$$

$\mathbf{d}_M(\nu)$ is defined by $\mathbf{d}_N(\mu)$ with N, μ replaced by M, ν respectively.

The real valued N *x* M array satisfies

$$\tan\left(\frac{\mu}{2}\right)\mathbf{K}_1\mathbf{D}(\mu,\nu) = \mathbf{K}_2\mathbf{D}(\mu,\nu) \quad (13)$$

where $\mathbf{K}_1$ and $\mathbf{K}_2$ are the real and imaginary parts of $\mathbf{Q}_{N-1}^H\mathbf{J}_2\mathbf{Q}_N^H$, $\mathbf{J}_2$ select the last *N-1* elements of an *N x 1* vector.

The *NM x 1* real valued manifold in vector form $\mathbf{d}(\mu,\nu) = vec[\mathbf{D}(\mu,\nu)]$ satisfies the requirement

$$\tan\left(\frac{\mu}{2}\right)\mathbf{K}_{\mu 1}\mathbf{D}(\mu,\nu)=\mathbf{K}_{\mu 2}\mathbf{D}(\mu,\nu) \quad (14)$$

where $\mathbf{K}_{\mu 1}$ and $\mathbf{K}_{\mu 2}$ are the *(N-1)M x NM* matrices

$$\mathbf{K}_{\mu 1}=\mathbf{I}_M\otimes\mathbf{K}_1,\ \mathbf{K}_{\mu 2}=\mathbf{I}_M\otimes\mathbf{K}_2 \quad (15)$$

where $\otimes$ denotes the Kronecker matrix product.

Similarly, $\mathbf{K}_3\mathbf{d}_M(\nu)=\mathbf{K}_4\mathbf{d}_M(\nu)$

where $\mathbf{K}_3=\mathrm{Re}\{\mathbf{Q}_{M-1}^H\mathbf{J}_2\mathbf{Q}_M\}$, $\mathbf{K}_4=\mathrm{Im}\{\mathbf{Q}_{M-1}^H\mathbf{J}_2\mathbf{Q}_M\}$

It follows that

$$\tan\left(\frac{\nu}{2}\right)\mathbf{D}(\mu,\nu)\mathbf{K}_3^T=\mathbf{D}(\mu,\nu)\mathbf{K}_4^T$$

$$\tan\left(\frac{\nu}{2}\right)\mathbf{K}_{\nu 1}\mathbf{d}(\mu,\nu)=\mathbf{K}_{\nu 2}\mathbf{d}(\mu,\nu) \quad (16)$$

where $\mathbf{K}_{\nu 1}$ and $\mathbf{K}_{\nu 2}$ are the *N(M-1) x NM* matrices

$$\mathbf{K}_{\nu 1}=\mathbf{K}_3\otimes\mathbf{I}_N,\ \mathbf{K}_{\nu 2}=\mathbf{K}_4\otimes\mathbf{I}_N \quad (17)$$

The real valued DOA matrix $\mathbf{D}=[\mathbf{d}(\mu_1,\nu_1),\ldots,\mathbf{d}(\mu_d,\nu_d)]$ satisfies

$$\mathbf{K}_{\mu 1}\mathbf{D}\boldsymbol{\Omega}_\mu=\mathbf{K}_{\mu 2}\mathbf{D} \quad (18)$$

where

$$\boldsymbol{\Omega}_\mu=diag\left\{\tan\left(\frac{\mu_1}{2}\right),\ldots,\tan\left(\frac{\mu_d}{2}\right)\right\},\ \mathbf{K}_{\nu 1}\mathbf{D}\boldsymbol{\Omega}_\nu=\mathbf{K}_{\nu 2}\mathbf{D} \quad (19)$$

where $\boldsymbol{\Omega}_\nu=diag\left\{\tan\left(\frac{\nu_1}{2}\right),\ldots,\tan\left(\frac{\nu_d}{2}\right)\right\}$

If $\mathbf{X}$ denotes the *NM x* N_s complex valued element space data matrix, the array output data matrix may be expressed as $\mathbf{Y}=\left(\mathbf{Q}_M^H\otimes\mathbf{Q}_N^H\right)\mathbf{X}$ and the appropriate *NM x d* signal eigenvector matrix $\mathbf{E}_s$ may be computed as the *d* "largest" left singular vectors of [Re{**Y**}, Im{**Y**}]. Viewing the signal relations as

$$\mathbf{K}_{\mu 1}\mathbf{E}_s\boldsymbol{\psi}_\mu=\mathbf{K}_{\mu 2}\mathbf{E}_s \text{ where } \boldsymbol{\psi}_\mu=\mathbf{T}^{-1}\boldsymbol{\Omega}_\mu\mathbf{T} \quad (20)$$

$$\mathbf{K}_{\nu 1}\mathbf{E}_s\boldsymbol{\psi}_\nu=\mathbf{K}_{\nu 2}\mathbf{E}_s \text{ where } \boldsymbol{\psi}_\nu=\mathbf{T}^{-1}\boldsymbol{\Omega}_\nu\mathbf{T} \quad (21)$$

Finally, from the eigenvalues of the matrix $\boldsymbol{\psi}_\mu+j\boldsymbol{\psi}_\nu=\mathbf{T}^{-1}\{\boldsymbol{\Omega}_\mu+j\boldsymbol{\Omega}_\nu\}\mathbf{T}$ compute spatial frequency estimates μ_i, ν_i.

This method provides closed form 2-D angle estimation in real time and has selfsame advantages as UCA-ESPRIT algorithm.

IV. Numerical examples for DOA estimation

The DOA estimation is investigated under the conditions of a UCA structure and URA structure with half-wavelength dipoles. Methods described above are utilized to perform the estimation [1]. The signal of interest (SOI) incomes from ($\theta=70^0,\phi=120^0$), while the three signals not of interest (SNOI) are directed from ($\theta=50^0,\phi=100^0$), ($\theta=45^0,\phi=95^0$), and ($\theta=90^0,\phi=140^0$) are given in Table I and Table III. The signal-to-noise ratio in all the considered cases is assumed to be (- 40) dB.

The results from UCA simulations are presented in Table II. The UCA with radius $a=0.6\lambda$ is examined about two scenarios: a) when array consists of *N=6* elements; b) when array consists of *N=8* elements.

The results from simulations for URA are described in Table IV. Two configurations of URA are examined: a) a (*N*=6, *M*=6) elements uniform rectangular array with $d_x=d_y=0.6\lambda$; b) a (*N*=8, *M*=8) elements uniform rectangular array with $d_x=d_y=0.6\lambda$.

TABLE I

THE UCA-ESPRIT DOA DATA

	Case 1	Case 2
Number of elements	M=6	M=8
Interelement spacing	0.6λ	0.6λ
Number of incoming signals	1	1
Number of data samples	2000	2000
Actual		
SOI	$\theta_1=70^0$, $\varphi_1=120^0$	$\theta_1=70^0$, $\varphi_1=120^0$
SNOI 1	$\theta_2=50^0$, $\varphi_2=100^0$	$\theta_2=50^0$, $\varphi_2=100^0$
SNOI 2	$\theta_3=45^0$, $\varphi_3=95^0$	$\theta_3=45^0$, $\varphi_3=95^0$
SNOI 3	$\theta_4=90^0$, $\varphi_4=140^0$	$\theta_4=90^0$, $\varphi_4=140^0$

TABLE II

THE DOA ESTIMATIONS OBTAINED UTILIZING UCA-ESPRIT

	Case 1	Case 2
Number of elements	M=6	M=8
Interelement spacing	0.6λ	0.6λ
Number of incoming signals	1	1
Number of data samples	2000	2000
DOA Estimations		
SOI	$\theta_1=70.020^0$, $\varphi_1=120.054^0$	$\theta_1=69.991^0$, $\varphi_1=119.994^0$
SNOI 1	$\theta_2=50.057^0$, $\varphi_2=100.051^0$	$\theta_2=49.998^0$, $\varphi_2=99.992^0$
SNOI 2	$\theta_3=44.971^0$, $\varphi_3=94.963^0$	$\theta_1=44.991^0$, $\varphi_1=94.992^0$
SNOI 3	$\theta_4=90.015^0$, $\varphi_4=139.969^0$	$\theta_2=89.991^0$, $\varphi_2=139.992^0$

TABLE III

THE 2-D UNITARY ESPRIT DOA DATA

	Case 1	Case 2
Number of elements	M=6 ,N=6	M=8, N=8
Interelement spacing	0.6λ	0.6λ
Number of incoming signals	1	1
Number of data samples	2000	2000
Actual		
SOI	$\theta_1=70^0$, $\varphi_1=120^0$	$\theta_1=70^0$, $\varphi_1=120^0$
SNOI 1	$\theta_2=50^0$, $\varphi_2=100^0$	$\theta_2=50^0$, $\varphi_2=100^0$
SNOI 2	$\theta_3=45^0$, $\varphi_3=95^0$	$\theta_3=45^0$, $\varphi_3=95^0$
SNOI 3	$\theta_4=90^0$, $\varphi_4=140^0$	$\theta_4=90^0$, $\varphi_4=140^0$

TABLE IV

THE DOA ESTIMATIONS OBTAINED USING 2-D UNITARY ESPRIT

	Case 1	Case 2
Number of elements	M=6 ,N=6	M=8, N=8
Interelement spacing	0.6λ	0.6λ
Number of incoming signals	1	1
Number of data samples	2000	2000
DOA Estimations		
SOI	$\theta_1=70.018^0$, $\varphi_1=120.051^0$	$\theta_1=69.994^0$, $\varphi_1=119.995^0$
SNOI 1	$\theta_2=50.055^0$, $\varphi_2=100.046^0$	$\theta_2=49.995^0$, $\varphi_2=99.995^0$
SNOI 2	$\theta_3=44.973^0$, $\varphi_3=94.966^0$	$\theta_3=44.983^0$, $\varphi_3=94.997^0$
SNOI 3	$\theta_4=90.018^0$, $\varphi_4=139.973^0$	$\theta_4=89.992^0$, $\varphi_4=139.998^0$

Both types of arrays are investigated in the presence of the Additive White Gaussian Noise (AWGN) with the zero mean, and variance 0.1. The results demonstrate theirs ability for accurate estimation, great performance, and robustness.

V. CONCLUSION

This paper investigated uniform circular and rectangular smart antennas with half-wavelength dipoles. A brief theory of two different antenna arrays to distinguish the direction of arrival by ESPRIT algorithm is considered. This theory was supported by suitable numerical data (see the Tables). The antennas were exploited in order to obtain more efficient method for a calculation of accurate DOA of impinging signals at the array.

Numerical examples have illustrated that the optimal scenario for the antenna geometry is UCA with *M*=6 elements, because of the symmetry UCA has almost the same performance as URA but with lower number of elements.

ACKNOWLEDGEMENT

Project no. 21 "Improvement of the research potential in the area of engineering and information technology" in the frame of Program "Development of human resources" and Ministry of Education of Bulgaria.

REFERENCES

[1] M. Zoltowski et al., “Closed-Form 2-D Angle Estimation with Rectangular Arrays in Element Space or Beamspace via Unitary ESPRIT”, IEEE Transactions on Signal Processing, vol. 44, no. 2, pp. 316-328, 1996.

[2] R. Roy, T. Kailath, "ESPRIT-Estimation of Signal Parameters via Rotational Invariance Techniques", IEEE Transactions on Acoustics, Speech, and Signal Processing, vol. 37, no. 7, pp. 984-995, 1989.

[3] L. C. Godara, “Smart Antennas”, CRC Press LLC, Florida, 2004.

[4] N. Herscovici, C. Christodoulou, "Uniform Circular Arrays for Smart Antennas", IEEE Antennas and Propagation Magazine, vol. 47, no. 4, pp. 192-206, 2005.

[5] C. Mathews, M. Zoltowski, “Eigenstructure for 2-D Angle Estimation with Uniform Circular Arrays”, IEEE Transactions on Signal Processing, vol. 42, no. 9, pp. 2395-2407, 1994.

[6] S. Bellofiore et al., “Smart-antenna systems for mobile communication networks, part 1: overview and antenna design”, IEEE Antennas and Propag. Magazine, vol. 44, pp. 106-114, 2002.

[7] K. Lonngren, S. Savov, “Fundamentals of Electromagnetics with Matlab”, SciTech, 2005.